Computation of nonlinear ultrasound fields using a linearized contrast source method

Martin D. Verweij,[a] Libertario Demi, and Koen W. A. van Dongen
Laboratory of Acoustical Wavefield Imaging, Department of Imaging Science and Technology, Faculty of Applied Sciences, Delft University of Technology, Lorentzweg 1, 2628 CD Delft, The Netherlands

(Received 7 February 2012; revised 23 July 2012; accepted 29 August 2012)

Nonlinear ultrasound is important in medical diagnostics because imaging of the higher harmonics improves resolution and reduces scattering artifacts. Second harmonic imaging is currently standard, and higher harmonic imaging is under investigation. The efficient development of novel imaging modalities and equipment requires accurate simulations of nonlinear wave fields in large volumes of realistic (lossy, inhomogeneous) media. The Iterative Nonlinear Contrast Source (INCS) method has been developed to deal with spatiotemporal domains measuring hundreds of wavelengths and periods. This full wave method considers the nonlinear term of the Westervelt equation as a nonlinear contrast source, and solves the equivalent integral equation via the Neumann iterative solution. Recently, the method has been extended with a contrast source that accounts for spatially varying attenuation. The current paper addresses the problem that the Neumann iterative solution converges badly for strong contrast sources. The remedy is linearization of the nonlinear contrast source, combined with application of more advanced methods for solving the resulting integral equation. Numerical results show that linearization in combination with a Bi-Conjugate Gradient Stabilized method allows the INCS method to deal with fairly strong, inhomogeneous attenuation, while the error due to the linearization can be eliminated by restarting the iterative scheme. © *2013 Acoustical Society of America*. [http://dx.doi.org/10.1121/1.4812863]

PACS number(s): 43.25.Jh, 43.25.Cb, 43.35.Bf, 43.80.Qf [NAS] Pages: 1442–1453

I. INTRODUCTION

In medical diagnostic ultrasound there is a continuing interest in nonlinear acoustics because it provides various opportunities to improve image quality.[1] Usually, these improvements are due to the gradual generation of higher harmonics of the fundamental frequency band occupied by the emitted signal. For more than a decade, diagnostic sonography of tissue is based on the reflections of the second harmonic instead of the fundamental, because this approach improves the resolution and reduces the clutter due to near field and grating lobe artifacts.[1–3] More recently, it has been shown that the performance may be further improved by using the combined reflections from the third, fourth, and fifth harmonic.[4–6] Untargeted[7] and targeted[8] microbubbles are used for contrast enhancement of blood and for molecular imaging, respectively. The presence of bubbles causes a strong increase of the nonlinear behavior of the solution, and imaging of the bubble population is either performed at a higher harmonic[9,10] or at the subharmonic,[11] i.e., half the fundamental frequency. In the context of contrast enhanced ultrasound, there has also been a recent interest in the phenomenon of self-demodulation,[12] which involves the frequency band below the fundamental. Exploitation of the possibilities of nonlinear acoustics requires the development of novel imaging modalities and devices. Due to the nonlinear nature of the involved phenomena, this cannot be done without accurate numerical simulations of the nonlinear acoustic wave fields that are involved.

Existing methods for the numerical simulation of nonlinear acoustic wave fields fall either in the category of forward wave methods or in the category of full wave methods.[13,14] Forward wave methods start with the pressure distribution in the plane of the transducer, and march the field forward in a preferred direction that usually corresponds to the propagation direction of the main part of the field.[15–22] All these methods use the solution of the one-dimensional (1D) Burgers equation[23] to perform the substep that accounts for the nonlinearity. Many methods, such as the KZK method,[17,21] also subject the acoustic wave equation to a parabolic approximation. Due to these facts, forward wave methods are inaccurate for fields that (partly) propagate in directions that deviate from the preferred direction of propagation, and in particular these methods cannot deal with scattered wave fields.

Most full wave methods, on the other hand, solve the relevant basic acoustic equations by way of a Finite Difference method[24–26] or a Finite Element method,[27] and do not involve a preferred direction of propagation. Since these methods need at least ten points per smallest wavelength and per shortest period, the number of grid points for spanning a realistic computational domain soon becomes too large. The Iterative Nonlinear Contrast Source (INCS) method[28,29] was especially designed to avoid all these problems. It does not favor a particular direction of propagation, and since it only requires two points per wavelength or period, it can deal with nonlinear ultrasound fields over computational domains measuring hundreds of wavelengths and

[a]Author to whom correspondence should be addressed. Electronic mail: m.d.verweij@tudelft.nl

periods. Originally, the method could handle homogeneous nonlinear media with frequency power law attenuation.[28,30] Recently, the method has been extended to deal with media with spatially dependent nonlinearity and attenuation,[31,32] in which case its ability to deal with scattered wave fields becomes opportune.

The original INCS method[28,29] solves a version of the Westervelt equation.[23] The basic observation behind the method is that for weak to moderate nonlinearity, the quadratically nonlinear term in this equation has a relatively small influence on the total wave field. In view of this, the nonlinear term is considered as a nonlinear contrast source that, together with the primary source, operates in a linear background medium. Since the Green's function of this linear background medium is known, the total field can formally be found as the convolution of the Green's function and both sources. In this way, the problem has been recast into the form of an integral equation. The convolution is numerically performed as a multiplication in the wavevector-frequency domain, and filtering techniques are used to allow for a grid of only two points per wavelength and per period of the highest desired frequency.[33] For homogeneous media, the discretized integral equation is efficiently solved by the Neumann iterative solution.[33–37] Some other methods also employ the benefits of using the wavevector domain. However, unlike the INCS method, these methods either are not really omnidirectional[38–41] or require a dense sampling in the nonlinear case,[42] and none of these methods has a mechanism of iteratively improving the solution.

To extend the INCS method to inhomogeneous media, additional contrast sources may be introduced that account for the difference between the actual medium and the homogeneous background medium.[31,32,43] However, for stronger inhomogeneities the influences of these additional contrast sources need not be small, as opposed to the original nonlinear contrast source, and the Neumann iterative solution may become slowly convergent or even divergent. When this occurs, the solution of the integral equation by more advanced methods,[34–36,44] such as over-relaxation methods or Conjugate Gradient (CG) methods, becomes necessary. These advanced methods perform significantly better in case of inhomogeneous media. However, the nonlinear contrast source in the INCS method prohibits their direct application because, to the authors' knowledge, these methods are only applicable to linear integral equations. If this problem is not resolved, the INCS methods will not be suitable for dealing with stronger medium inhomogeneities.

The current paper describes how the INCS method may be adapted to allow for the application of advanced integral equation solvers. This will be achieved by linearization of the nonlinear contrast source with respect to the total wave field. The rationale behind this linearization is the same as that behind the INCS method itself, namely, that the total wave field may be considered as the sum of a linear primary contribution due to the primary source, and a secondary contribution due to the contrast sources. It is assumed that the square of the secondary contribution may be neglected. This effectively linearizes the nonlinear contrast source about the primary contribution, and enables the application of advanced methods for solving the remaining integral equation. Because the linearization reduces the spectral richness of the original nonlinear contrast source, it causes a systematic error that becomes significant for the higher harmonics. To counteract this effect, after a few iterations the linearization about the primary contribution may be replaced by a linearization about the total field obtained until then, and the scheme may be restarted. This restart strategy will be used to replenish the spectral content of the linearized contrast source and, in doing so, reduce the systematic error.

The theoretical developments of this paper are presented in Sec. II, which describes the basic equations, the INCS method, and the linearization process. Numerical results for lossless media and media with inhomogeneous losses are presented in Sec. III. These results show the influence of the linearization, the difference in performance between the Neumann iterative solution and the more advanced Bi-Conjugate Gradient Stabilized (Bi-CGSTAB) method, and the effect of the restart strategy. Conclusions on the presented research are given in Sec. IV.

II. THEORY

A. Wave equation

In this paper it is assumed that the nonlinear propagation of an acoustic pressure wave field $p = p(\boldsymbol{x}, t)$ in a homogeneous medium with attenuation is governed by the wave equation[28,30]

$$\nabla^2 p(\boldsymbol{x}, t) - \frac{1}{c_0^2}\partial_t^2 [m(t) *_t p(\boldsymbol{x}, t)] = -S_{\mathrm{pr}}(\boldsymbol{x}, t) - \frac{\beta}{\rho_0 c_0^4}\partial_t^2 p^2(\boldsymbol{x}, t). \tag{1}$$

Here c_0 and ρ_0 are the ambient speed of sound and the ambient volume density of mass of the medium. The function $m(t)$ is a causal compliance relaxation or memory function,[45–47] and $*_t$ denotes a temporal convolution, i.e.,

$$m(t) *_t p(\boldsymbol{x}, t) = \int_0^\infty m(t - t')p(\boldsymbol{x}, t')\mathrm{d}t'. \tag{2}$$

The relaxation function may be separated into

$$m(t) = \delta(t) + A(t), \tag{3}$$

where the Dirac delta function $\delta(t)$ represents the instantaneous behavior of the medium, and $A(t)$ is a causal relaxation function that represents the delayed reaction of the homogeneous medium on events that occurred in the past. The latter behavior is associated with the attenuation and the corresponding dispersion of the medium. The relaxation function formulation enables the modeling of many types of attenuation, among which the frequency power law losses that are exhibited by many biological tissues.[28,30,31,48–50] The coefficient of nonlinearity β indicates the degree of nonlinear behavior of the considered medium, and may be written as

$$\beta = 1 + \frac{B}{2A}, \tag{4}$$

where B/A is the parameter of nonlinearity of the medium. The term $S_{\mathrm{pr}}(\boldsymbol{x}, t)$ represents the primary source that generates the acoustic wave field. This term combines the source's volume density of volume injection rate $q(\boldsymbol{x}, t)$ and its volume density of volume force $\boldsymbol{f}(\boldsymbol{x}, t)$, according to

$$S_{\mathrm{pr}}(\boldsymbol{x}, t) = \rho_0 \partial_t q(\boldsymbol{x}, t) - \nabla \cdot \boldsymbol{f}(\boldsymbol{x}, t). \tag{5}$$

Equation (1) corresponds to the Westervelt equation,[23] except from application of the more general attenuation term instead of the usual thermoviscous loss term, and the introduction of the primary source term. The Westervelt equation is exact up until the terms of second order in the acoustic disturbance quantities, takes into account the global nonlinear effects, and neglects local nonlinear effects. Due to its similarity, the same facts apply to Eq. (1).

B. INCS method

The current paper considers the numerical solution of Eq. (1) by means of the INCS method.[28,29] This method is primarily designed to deal with weakly to moderately nonlinear behavior as encountered with, for example, diagnostic ultrasound. In this case, the influence of the nonlinear term is relatively small, and the total wave field may be considered as a combination of a linear primary contribution and a lesser, nonlinear secondary contribution. To facilitate this point of view, Eq. (1) is rewritten as

$$\begin{aligned} &\nabla^2 p(\boldsymbol{x}, t) - \frac{1}{c_0^2} \partial_t^2 [m(t) *_t p(\boldsymbol{x}, t)] \\ &\quad = -S_{\mathrm{pr}}(\boldsymbol{x}, t) - S_{\mathrm{nl}}[p(\boldsymbol{x}, t)], \end{aligned} \tag{6}$$

where

$$S_{\mathrm{nl}}[p(\boldsymbol{x}, t)] = \frac{\beta}{\rho_0 c_0^4} \partial_t^2 p^2(\boldsymbol{x}, t), \tag{7}$$

is the nonlinear term of Eq. (1). If $S_{\mathrm{nl}}[p(\boldsymbol{x}, t)]$ were absent, Eq. (6) would be a linear wave equation, and the primary source $S_{\mathrm{pr}}(\boldsymbol{x}, t)$ would generate a linear wave field. This is the assumed linear primary contribution to the total wave field. With the INCS method, $S_{\mathrm{nl}}[p(\boldsymbol{x}, t)]$ gets the role of a separate source. This source is called a contrast source and it accounts for the difference between the linear and the nonlinear case, i.e., it generates the nonlinear correction wave field that forms the secondary contribution to the total wave field. The nonlinear contrast source depends on the total wave field itself, and is distributed over the entire space. Since the wave operator at the left-hand side of Eq. (6) applies to a linear medium, both the primary source and the nonlinear contrast source may be thought to operate in a linear background medium. This implies that the fields of the primary source and the contrast source may be computed using the same techniques that apply to a linear medium. Now suppose that the Green's function of the background medium, i.e., the function $G(\boldsymbol{x}, t)$ that satisfies

$$\nabla^2 G(\boldsymbol{x}, t) - \frac{1}{c_0^2} \partial_t^2 [m(t) *_t G(\boldsymbol{x}, t)] = -\delta(\boldsymbol{x}) \delta(t), \tag{8}$$

is known. In the lossless case, the closed form expression of the Green's function in the space-time domain is known to be[51]

$$G(\boldsymbol{x}, t) = \frac{\delta(t - \|\boldsymbol{x}\| / c_0)}{4\pi \|\boldsymbol{x}\|}, \tag{9}$$

where $\|\boldsymbol{x}\|$ is the length of $\boldsymbol{x}$. In case of attenuation, the Green's function may most conveniently be presented in the space-frequency domain as

$$\hat{G}(\boldsymbol{x}, \omega) = \frac{\exp[-\gamma(\omega) \|\boldsymbol{x}\|]}{4\pi \|\boldsymbol{x}\|}, \tag{10}$$

where $\gamma(\omega) = \alpha(\omega) + j\beta(\omega)$, with $\alpha(\omega)$ being the attenuation coefficient and $\beta(\omega)$ being the phase coefficient. These functions account for the attenuation and the dispersion of the medium, respectively, and may be chosen to model power law attenuation as encountered in biological tissue.[28,30,31,52] Because the Green's function describes the spatiotemporal impulse response of the relevant linear background medium, the solution of Eq. (6) may formally be written as

$$p(\boldsymbol{x}, t) = G(\boldsymbol{x}, t) *_{\boldsymbol{x},t} \{S_{\mathrm{pr}}(\boldsymbol{x}, t) + S_{\mathrm{nl}}[p(\boldsymbol{x}, t)]\}, \tag{11}$$

in which $*_{\boldsymbol{x},t}$ denotes the spatiotemporal convolution

$$\begin{aligned} &G(\boldsymbol{x}, t) *_{\boldsymbol{x},t} \{S_{\mathrm{pr}}(\boldsymbol{x}, t) + S_{\mathrm{nl}}[p(\boldsymbol{x}, t)]\} \\ &\quad = \int_{\mathcal{T}} \int_{\mathcal{D}} G(\boldsymbol{x} - \boldsymbol{x}', t - t') \\ &\qquad \times \{S_{\mathrm{pr}}(\boldsymbol{x}', t') + S_{\mathrm{nl}}[p(\boldsymbol{x}', t')]\} \mathrm{d}\boldsymbol{x}' \mathrm{d}t'. \end{aligned} \tag{12}$$

Here, $\mathcal{T}$ and $\mathcal{D}$ are the relevant temporal and spatial domains of interest. Denoting the convolution of the Green's function and the primary source by $p^{(0)}(\boldsymbol{x}, t)$, Eq. (11) may be rewritten as

$$p(\boldsymbol{x}, t) = p^{(0)}(\boldsymbol{x}, t) + G(\boldsymbol{x}, t) *_{\boldsymbol{x},t} S_{\mathrm{nl}}[p(\boldsymbol{x}, t)]. \tag{13}$$

The terms $p^{(0)}(\boldsymbol{x}, t)$ and $G(\boldsymbol{x}, t) *_{\boldsymbol{x},t} S_{\mathrm{nl}}[p(\boldsymbol{x}, t)]$ are the linear primary contribution due to the primary source and the nonlinear secondary contribution due to the contrast source, respectively. Since the nonlinear contrast source depends on the total acoustic pressure field $p(\boldsymbol{x}, t)$, Eq. (13) is an integral equation.

The main observation behind the INCS method is that for weakly to moderately nonlinear behavior the secondary contribution due to the contrast source is relatively small. In that case, an intuitive way to obtain increasingly accurate approximations of the total pressure wave field is to compute the linear primary field contribution $p^{(0)}(\boldsymbol{x}, t)$, using this to obtain a first approximation for the contrast source $S_{\mathrm{nl}}[p(\boldsymbol{x}, t)]$, then compute a first approximation of the total field $p(\boldsymbol{x}, t)$, and successively repeat the last two steps. This results in the Neumann iterative solution

$$p^{(0)}(\boldsymbol{x}, t) = G(\boldsymbol{x}, t) *_{\boldsymbol{x},t} S_{\mathrm{pr}}(\boldsymbol{x}, t), \tag{14}$$

$$p^{(j)}(\boldsymbol{x}, t) = p^{(0)}(\boldsymbol{x}, t) + G(\boldsymbol{x}, t) *_{\boldsymbol{x},t} S_{\mathrm{nl}}[p^{(j-1)}(\boldsymbol{x}, t)] \quad (j \geq 1), \tag{15}$$

where the notation $p^{(j)}(\boldsymbol{x}, t)$ is used to indicate the jth iteration. The most involving task in the numerical evaluation of the scheme is the spatiotemporal convolution, which is efficiently performed with the Filtered Convolution method.[33] The method first filters out all spatial and temporal frequencies above the highest frequencies of interest. This enables sampling at only two points per shortest period or shortest wavelength, without introducing aliasing. Then the resulting four-dimensional discrete convolution is performed using Fast Fourier Transforms.

C. Linearization of the contrast source

The Neumann iterative solution in Eqs. (14) and (15) is a particular way to solve the integral equation in Eq. (13).[33–37] In case of homogeneous media, as considered until now, the only term in the contrast source is $S_{\mathrm{nl}}[p(\boldsymbol{x}, t)]$. As long as the influence of this term is small, as in the case of weakly to moderately nonlinear behavior, the Neumann iterative solution is expected to converge quite fast. This behavior is confirmed in practice.[28,29]

However, in case of inhomogeneous media the situation may become more complex. For example, in media with inhomogeneous losses the propagation of the acoustic pressure wave field is governed by the wave equation[31,32,43]

$$\nabla^2 p(\boldsymbol{x}, t) - \frac{1}{c_0^2}\partial_t^2[m(\boldsymbol{x}, t) *_t p(\boldsymbol{x}, t)] = -S_{\mathrm{pr}}(\boldsymbol{x}, t) - S_{\mathrm{nl}}[p(\boldsymbol{x}, t)], \tag{16}$$

with

$$m(\boldsymbol{x}, t) = \delta(t) + A_{\mathrm{bg}}(t) + \Delta A(\boldsymbol{x}, t) = m_{\mathrm{bg}}(t) + \Delta A(\boldsymbol{x}, t). \tag{17}$$

Here, the relaxation function $A_{\mathrm{bg}}(t)$ represents the attenuation in the homogeneous background medium, and the relaxation function $\Delta A(\boldsymbol{x}, t)$ accounts for the difference in the loss between the actual medium and the background medium. A straightforward application of the INCS method in Sec. II B requires knowledge of the Green's function of the linear but inhomogeneous background, i.e., the function $G(\boldsymbol{x}, t)$ that satisfies

$$\nabla^2 G(\boldsymbol{x}, t) - \frac{1}{c_0^2}\partial_t^2[m(\boldsymbol{x}, t) *_t G(\boldsymbol{x}, t)] = -\delta(\boldsymbol{x})\delta(t). \tag{18}$$

In general, it will not be possible to find the required Green's function in closed form, and the numerical solution of the equation above may be as involving as generating the Neumann iterative solution itself. One way to overcome this difficulty is to return to a homogeneous background medium by writing Eq. (16) as

$$\nabla^2 p(\boldsymbol{x}, t) - \frac{1}{c_0^2}\partial_t^2[m_{\mathrm{bg}}(t) *_t p(\boldsymbol{x}, t)] = -S_{\mathrm{pr}}(\boldsymbol{x}, t) - S_{\mathrm{nl}}[p(\boldsymbol{x}, t)] - S_{\mathrm{at}}[p(\boldsymbol{x}, t)], \tag{19}$$

with

$$S_{\mathrm{at}}[p(\boldsymbol{x}, t)] = -\frac{1}{c_0^2}\partial_t^2[\Delta A(\boldsymbol{x}, t) *_t p(\boldsymbol{x}, t)]. \tag{20}$$

This term is an additional contrast source that accounts for the inhomogeneous losses of the medium,[31,32,43] and can easily be incorporated in the INCS method as described in Sec. II B. In this case the counterpart of Eq. (13) becomes

$$p(\boldsymbol{x}, t) = p^{(0)}(\boldsymbol{x}, t) + G(\boldsymbol{x}, t) *_{\boldsymbol{x},t}\{S_{\mathrm{nl}}[p(\boldsymbol{x}, t)] + S_{\mathrm{at}}[p(\boldsymbol{x}, t)]\}, \tag{21}$$

in which $G(\boldsymbol{x}, t)$ satisfies Eq. (8) with $m(t) = m_{\mathrm{bg}}(t)$. Equation (21) may in principle be solved with a scheme that is similar to the Neumann iterative solution in Eqs. (14) and (15).

The above approach offers a straightforward way to account for various medium behaviors that deviate from a linear homogeneous background medium. However, the contributions of the additional contrast sources, as opposed to the original nonlinear contrast source $S_{\mathrm{nl}}[p(\boldsymbol{x}, t)]$, need *not* always be small. As a consequence the Neumann iterative solution in Eqs. (14) and (15) may become slowly convergent or even divergent. Fortunately, there exist more advanced methods,[34–36] like over-relaxation methods, CG methods, etc., for solving integral equations of the form

$$p(\boldsymbol{x}, t) = p^{(0)}(\boldsymbol{x}, t) + G(\boldsymbol{x}, t) *_{\boldsymbol{x},t} S_{\mathrm{cs}}[p(\boldsymbol{x}, t)], \tag{22}$$

where $S_{\mathrm{cs}}[p(\boldsymbol{x}, t)]$ represents all the relevant contrast sources. In case of medium inhomogeneities, these advanced methods usually offer a better convergence than the Neumann iterative solution, as demonstrated for the linear case.[34–36,44] Unfortunately, the application of these methods in the nonlinear context of the INCS method is prohibited because, to the authors' knowledge, these methods are only suited for the solution of linear integral equations. This implies that in Eq. (22) the contrast source $S_{\mathrm{cs}}[p(\boldsymbol{x}, t)]$ must be linear in $p(\boldsymbol{x}, t)$. Although contrast sources like $S_{\mathrm{at}}[p(\boldsymbol{x}, t)]$ that represent the medium inhomogeneities are usually linear in $p(\boldsymbol{x}, t)$, in the current situation $S_{\mathrm{cs}}[p(\boldsymbol{x}, t)]$ is nonlinear because it also contains the nonlinear contrast source $S_{\mathrm{nl}}[p(\boldsymbol{x}, t)]$.

To overcome this restriction of the INCS method, now the nonlinear contrast source will be linearized. This linearization is based on the same observation that underlies the INCS method itself, i.e., that the total acoustic wave field $p(\boldsymbol{x}, t)$ may be considered as a combination of a linear primary contribution $p^{(0)}(\boldsymbol{x}, t)$ and a secondary contribution $\tilde{p}(\boldsymbol{x}, t)$, i.e.,

$$p(\boldsymbol{x}, t) = p^{(0)}(\boldsymbol{x}, t) + \tilde{p}(\boldsymbol{x}, t). \tag{23}$$

Under the assumption that $\tilde{p}^2(\boldsymbol{x}, t)$ may be neglected, $p^2(\boldsymbol{x}, t)$ can be approximated by

$$p^2(\boldsymbol{x},t) \approx [p^{(0)}(\boldsymbol{x},t)]^2 + 2p^{(0)}(\boldsymbol{x},t)\tilde{p}(\boldsymbol{x},t) = -[p^{(0)}(\boldsymbol{x},t)]^2 + 2p^{(0)}(\boldsymbol{x},t)p(\boldsymbol{x},t). \quad (24)$$

Using this result in Eq. (7), the linearized version of Eq. (21) becomes

$$p(\boldsymbol{x},t) = p^{(0)}(\boldsymbol{x},t) + G(\boldsymbol{x},t) *_{\boldsymbol{x},t}\{S_{\mathrm{nl}}^{\mathrm{new}}[p(\boldsymbol{x},t)] + S_{\mathrm{at}}[p(\boldsymbol{x},t)]\}, \quad (25)$$

where

$$S_{\mathrm{nl}}^{\mathrm{new}}(\boldsymbol{x},t) = \frac{\beta}{\rho_0 c_0^4}\partial_t^2\{-[p^{(0)}(\boldsymbol{x},t)]^2 + 2p^{(0)}(\boldsymbol{x},t)p(\boldsymbol{x},t)\}. \quad (26)$$

The primary wave field $p^{(0)}(\boldsymbol{x},t)$ that appears in these equations is easily computed as the zero-order term of the Neumann iterative solution. Since all contrast sources in Eq. (25) are linear in $p(\boldsymbol{x},t)$, this integral equation may be solved by any appropriate method.

D. Restart strategy

For a given wave field $p(\boldsymbol{x},t)$, omission of the square of $\tilde{p}(\boldsymbol{x},t)$ in Eq. (24) causes a reduction of the spectral width of the nonlinear contrast source. It may be shown that this increasingly disturbs the harmonics of higher order. However, in the Appendix it is explained that, as far as the linearization process is concerned, the primary wave field $p^{(0)}(\boldsymbol{x},t)$ may be replaced by any other known field that forms a close approximation to the total wave field $p(\boldsymbol{x},t)$. This implies that the adverse effect of the linearization may be counteracted by replacing, say after J iterations, $p^{(0)}(\boldsymbol{x},t)$ by $p^{(J)}(\boldsymbol{x},t)$ in Eq. (26), and restarting the scheme. Since the spectral content of $p^{(J)}(\boldsymbol{x},t)$ is much wider than that of $p^{(0)}(\boldsymbol{x},t)$, this restart strategy will replenish the spectral content of the linearized contrast source and thus reduce the systematic error due to linearization.

III. NUMERICAL RESULTS

Several numerical studies will be presented that show the consequences of linearizing the contrast source, using the Bi-CGSTAB method[53] as an alternative method (besides the Neumann iterative solution) for solving the resulting integral equation, and applying the restart strategy for eliminating the systematic error.

The Bi-CGSTAB method solves the discrete version of the integral equation

$$L[u(\boldsymbol{x}',t'),\boldsymbol{x},t] = f(\boldsymbol{x},t), \quad (27)$$

where $L[u,\boldsymbol{x},t]$ is a known integral operator, $f(\boldsymbol{x},t)$ is a known function, and $u(\boldsymbol{x}',t')$ is the unknown function to be found. This implies that Eq. (25) should be recast in the form of Eq. (27). This is achieved by taking $u(\boldsymbol{x}',t') = p(\boldsymbol{x}',t'), f(\boldsymbol{x},t) = p^{(0)}(\boldsymbol{x},t)$, and

$$L[u(\boldsymbol{x}',t'),\boldsymbol{x},t] = u(\boldsymbol{x},t) - \int_{\mathcal{T}}\int_{\mathcal{D}} G(\boldsymbol{x}-\boldsymbol{x}',t-t') \times \{S_{\mathrm{nl}}^{\mathrm{new}}[u(\boldsymbol{x}',t')] + S_{\mathrm{at}}[u(\boldsymbol{x}',t')]\}\mathrm{d}\boldsymbol{x}'\mathrm{d}t'. \quad (28)$$

In all cases, the acoustic wave field is generated by a source that generates a Gaussian modulated surface pressure

$$p(t) = P_0 \exp[-(2t/t_{\mathrm{w}})^2]\sin(2\pi f_0 t), \quad (29)$$

with a pressure amplitude $P_0 = 1\,\mathrm{MPa}$, a center frequency $f_0 = 1\,\mathrm{MHz}$, and a pulse width $t_{\mathrm{w}} = 3/f_0$. In the numerical studies that involve a three-dimensional (3D) beam, the source is a 40 element phased array transducer, with elements measuring $w = 0.45\,\mathrm{mm}$ (width in the x direction) by $h = 10\,\mathrm{mm}$ (height in the y direction), and a pitch $d = 0.50\,\mathrm{mm}$. Elevation focusing is simulated to account for the effect of an acoustical lens. Unless noted otherwise, the transducer radiates in homogeneous lossless water with $\rho_0 = 998\,\mathrm{kg\,m^{-3}}$, $c_0 = 1482\,\mathrm{m\,s^{-1}}$, and $\beta = 3.52$.

The discretization of the INCS method is 2 points per wavelength and 2 points per period, both relating to a wave having a maximum frequency of interest of $(h+0.5)f_0$, where h is the order of the highest harmonic considered[29] ($h = 5$ in Secs. III A–III C, and $h = 3$ in Sec. III D).

Whenever an individual harmonic of order h is needed, this is obtained by filtering the total wave field with an eighth order Butterworth filter with cutoff frequencies $(h \pm 0.4)f_0$; for the fundamental one should take $h = 1$.

A. 1D homogeneous configuration

First, a 1D homogeneous configuration is considered, in which the source is located at $z = 0\,\mathrm{mm}$ and the pressure at $z = 100\,\mathrm{mm}$ is computed. This distance is shorter than the shock formation distance $\bar{z} = 150\,\mathrm{mm}$ for a monofrequency signal with frequency f_0.

Figure 1 shows the frequency spectra of the pressure pulses, as obtained for successive iterations under different scenarios. These spectra are compared to the spectrum of the solution of the Burgers equation,[23] which in the 1D case provides the exact solution under the same conditions that apply for the Westervelt equation.[54]

The top panel of Fig. 1 shows the behavior of the original INCS method, i.e., using the Neumann iterative solution without linearization of the contrast source. This scheme converges quickly, and the results for iterations $j \geq 5$ are visually indistinguishable from the result of the Burgers solution. Results in the center panel apply to the combination of the Neumann iterative solution and a linearized contrast source. In this case, the scheme converges a little slower, and the differences between the successive iterations become visually indistinguishable for iterations $j \geq 6$. Moreover, this converged result does not coincide with the Burgers result. The bottom panel shows the behavior of the combination of the Bi-CGSTAB method and a linearized contrast source. This scheme converges even quicker as the original INCS method, with successive iterations being visually indistinguishable for $j \geq 4$. However, the converged result again does not coincide with the Burgers result.

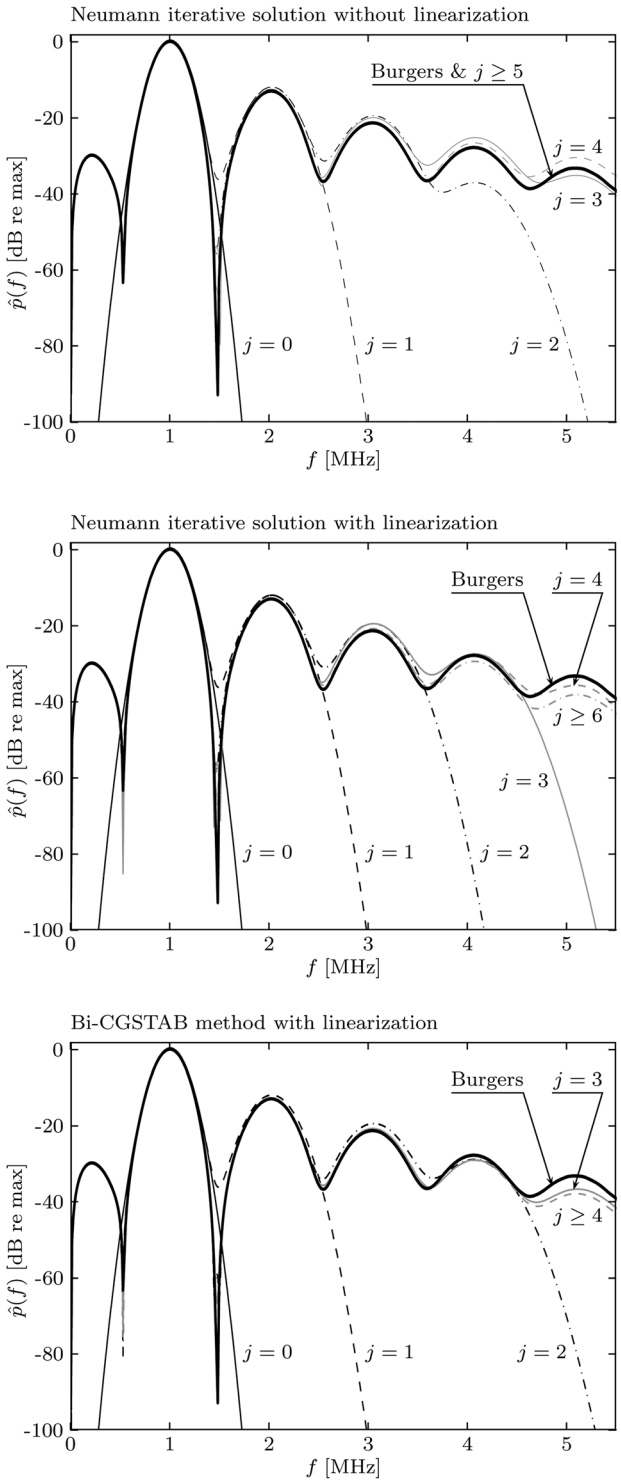

FIG. 1. Spectra of the iterations obtained for the 1D case by (top) the Neumann iterative solution without linearization, (center) the Neumann iterative solution with linearization, and (bottom) the Bi-CGSTAB method with linearization. The thick solid line indicates the result obtained from the Burgers equation, and j is the iteration number.

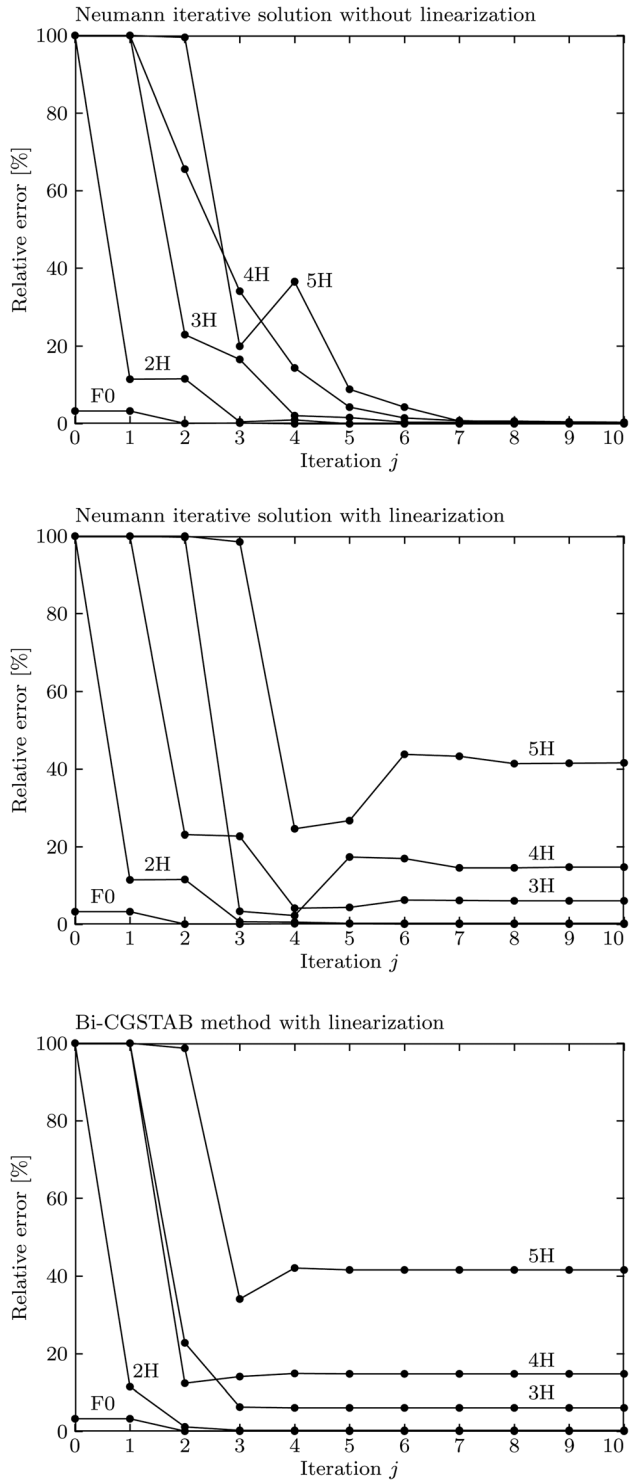

FIG. 2. The relative error in the harmonics obtained for the 1D case by (top) the Neumann iterative solution without linearization, (center) the Neumann iterative solution with linearization, and (bottom) the Bi-CGSTAB method with linearization. The error is determined with respect to the solution of the Burgers equation.

Upon comparing the different schemes, three observations may be made. First, while the linearization seems to have an adverse effect on the convergence of the Neumann iterative solution, this effect is more than compensated by using the more advanced Bi-CGSTAB method. So a scheme with linearization may run even faster as the original INCS method. Second, both schemes with linearization converge to the same result, which does not entirely coincide with the Burgers result. Thus linearization causes a systematic error that is independent of the applied method for solving the integral equation. Third, after convergence has been obtained, linearization only seems to have a noticeable effect on the fourth and higher harmonics and, since these are small, will have a small effect on the total nonlinear wave field.

The observations made above are confirmed by Fig. 2, which for each scenario shows the development of the relative error in the harmonics. The relative error in the hth harmonic of the jth iteration is in this case defined as

$$\text{Error} = \frac{|\hat{p}^{(j)}(hf_0) - \hat{p}^{\text{B}}(hf_0)|}{|\hat{p}^{\text{B}}(hf_0)|}. \tag{30}$$

Here, $\hat{p}^{(j)}(hf_0)$ indicates the spectral component of the jth iteration at the single frequency hf_0, and $\hat{p}^{\text{B}}(hf_0)$ denotes the corresponding spectral component of the Burgers solution. Notice that in the center and bottom panels the errors for the highest iterations are the same, indicating that the systematic error is caused by the linearization and not by the choice of the method for solving the integral equation.

B. 3D homogeneous configuration with an unsteered beam

Here, a 3D homogeneous configuration is considered, in which a phased array at $z = 0$ mm generates an unsteered beam, i.e., with a beam axis that makes an azimuthal angle of 0° with the z axis and an elevation angle of 90° with the y axis. The transducer is focused at $(x, y, z) = (0, 0, 35\,\text{mm})$, including elevation focusing. A computational domain with a size of $X \times Y \times Z = 30\,\text{mm} \times 20\,\text{mm} \times 50\,\text{mm}$ is used.

The left part of Fig. 3 shows the beam patterns in the plane $y = 0$ mm, for several harmonics. These results are obtained by the Neumann iterative solution in combination with a linearized contrast source. The scheme is iterated up to $j = 7$ (convergence), and the outcome is filtered to obtain the individual harmonics. Figure 3 clearly shows the typical features of the higher harmonic beam patterns that are generated by nonlinear propagation, such as the decrease of the focal width and the shift of the onset of the beams.

The right part of Fig. 3 depicts the patterns of the relative errors in the harmonics on the left. In these plots, the relative error in the hth harmonic is defined as

$$\text{Error} = \frac{|\max_t[p_h(\boldsymbol{x}, t)] - \max_t[p_h^{\text{N}}(\boldsymbol{x}, t)]|}{|\max_t[p_h^{\text{N}}(\boldsymbol{x}, t)]|}. \tag{31}$$

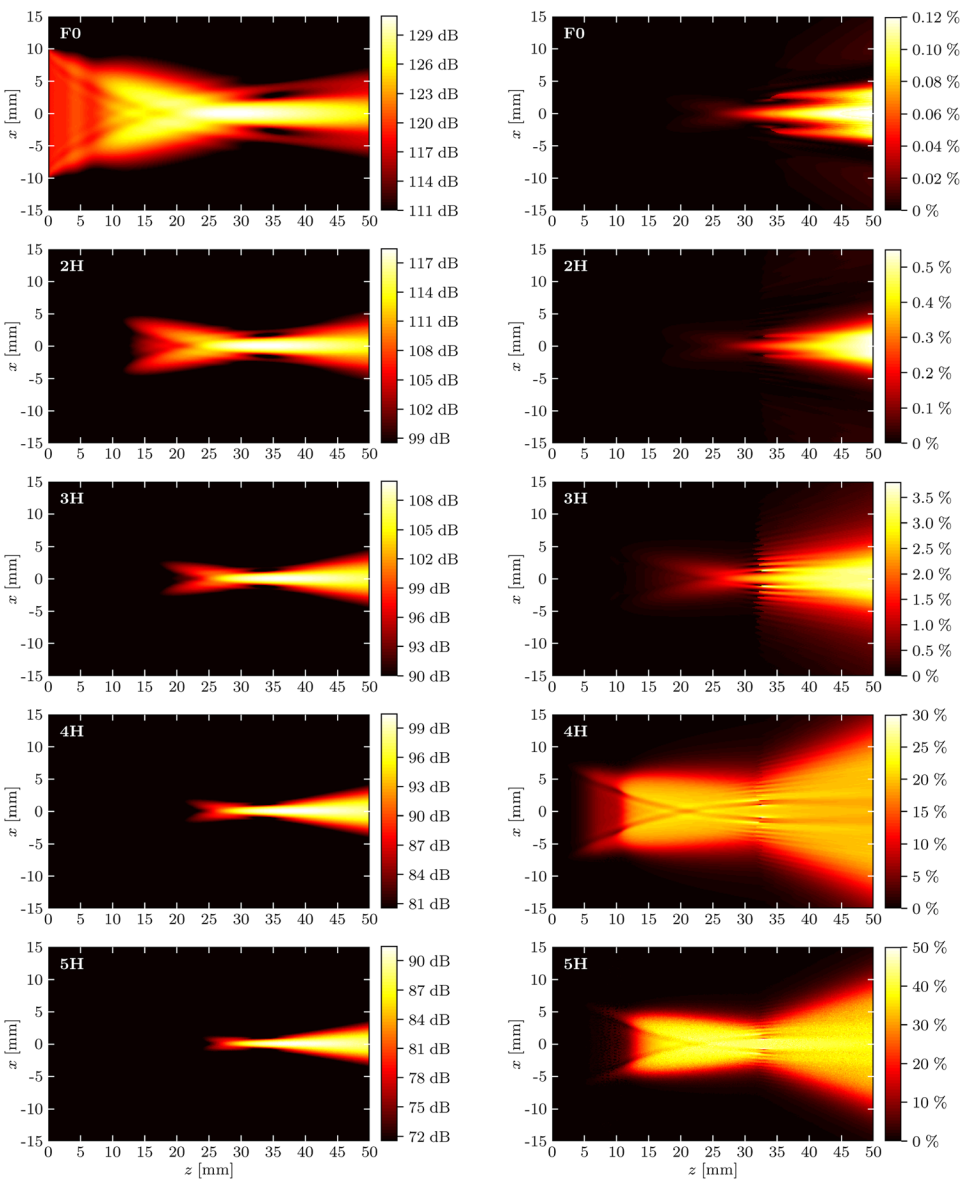

FIG. 3. (Color online) The unsteered beam patterns (left) and the relative errors (right) of the harmonics, obtained for the 3D case by the Neumann iterative solution with linearization. The error is determined with respect to the solution of the Neumann iterative solution without linearization of the contrast source. Both schemes are iterated up to $j = 7$ (convergence). Decibel values apply to the maximum field amplitude relative to a pressure of 1 Pa.

Here, $p_h(\boldsymbol{x}, t)$ is the hth harmonic obtained with the described method. The error is determined with respect to $p_h^{\mathrm{N}}(\boldsymbol{x}, t)$, which is the hth harmonic of the Neumann iterative solution without linearization of the contrast source, obtained for iteration $j = 7$ (convergence). The harmonics are extracted from the total signal by filtering. As before, it is observed in the figure that in general the errors increase for increasingly higher harmonics. A comparison of the relative errors in Fig. 3 with those in the center panel of Fig. 2 reveals that in the 3D case and the 1D case the systematic errors due to linearization are quite comparable. For the beams considered here, it may be observed that accurate results are obtained up until the third harmonic, while the error is high from the fourth harmonic onwards.

C. 3D homogeneous configuration with a steered beam

As the next case, a 3D homogeneous configuration is considered, in which the phased array at $z = 0$ mm generates a steered beam with a beam axis that makes an azimuthal angle of 45° with the z axis and an elevation angle of 90° with the y axis. The transducer is focused at $(x, y, z) = (35, 0, 35\,\mathrm{mm})$, including elevation focusing. A trapezoidal computational domain with a size of $X \times Y \times Z = 30\,\mathrm{mm} \times 20\,\mathrm{mm} \times 50\,\mathrm{mm}$ is used, having the same angles with respect to the y and z axes as the beam axis.

Figure 4 shows the beam profiles along the beam axis and along the line $(y, z) = (0, 35\,\mathrm{mm})$, for several harmonics. The results are in full correspondence with the results in Secs. III A and III B, and it may be concluded that linearization works equally well for a steered and an unsteered beam.

D. 3D configuration with inhomogeneous attenuation

Finally, the 3D inhomogeneous configuration of Fig. 5 is considered. The background medium is lossless water. The two spherical inclusions of radius $R = 2$ mm have the same ρ_0, c_0, and β as the background, but show a frequency power law attenuation[48–50] $\alpha = af^b$ with $a = 1.56\,\mathrm{Np\,cm^{-1}\,MHz^{-b}}$ and $b = 1.05$. Such losses can occur in bone, and may be considered extremely high in a biomedical context. The transducer is the same phased array as before, being located at $z = 0$ mm, and generating an unsteered beam that is focused at $(x, y, z) = (0, 0, 35\,\mathrm{mm})$, including elevation focusing. A computational domain with a size of $X \times Y \times Z = 30\,\mathrm{mm} \times 20\,\mathrm{mm} \times 50\,\mathrm{mm}$ is used.

Figure 6 shows the beam patterns in the plane $y = 0$ mm for several harmonics. The results are obtained by the Bi-CGSTAB method in combination with a linearized contrast source. The scheme is iterated up to $j = 7$ (convergence), and the outcome is filtered to obtain the individual harmonics. A comparison of the results with those in the left column of Fig. 3 shows that the originally symmetric beam patterns are deformed by the lossy inclusions. Note that the deformation becomes more prominent for the higher harmonics, although the overlap between the inclusions and the higher harmonic beams decreases. This effect may be explained by the nonlinear origin of the higher harmonics, which

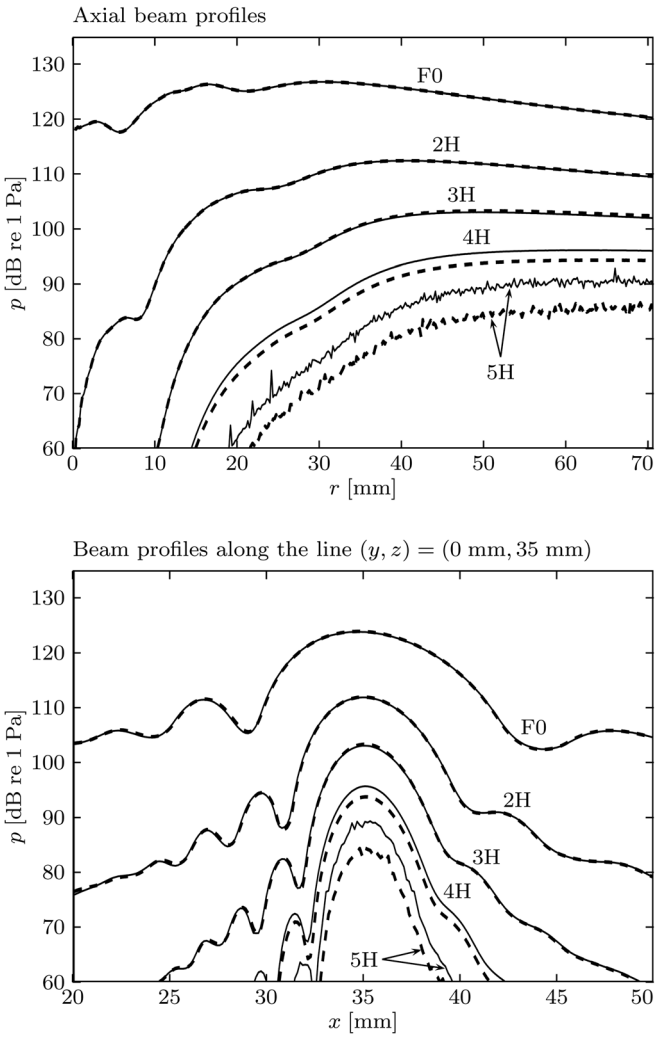

FIG. 4. Axial profiles (top) and profiles along the line $(y, z) = (0, 35\,\mathrm{mm})$ (bottom) of the harmonics of a steered beam. The profiles are obtained for the 3D case by the Neumann iterative solution without (solid line) and with (dashed line) linearization. Both schemes are iterated up to $j = 7$ (convergence). In the top panel, $r = (x^2 + z^2)^{1/2}$ is the distance along the beam axis.

makes that a slight disturbance in the fundamental becomes enhanced in the higher harmonics.

Figure 7 shows several snapshots of the total nonlinear wave field in the plane $y = 0$ mm. The results are again obtained by using $j = 7$ iterations of the Bi-CGSTAB method combined with a linearized contrast source. The snapshot at

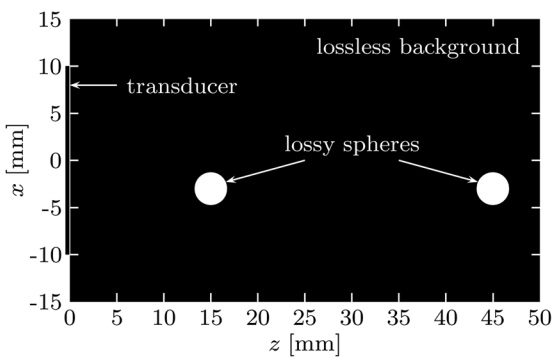

FIG. 5. The inhomogeneous configuration.

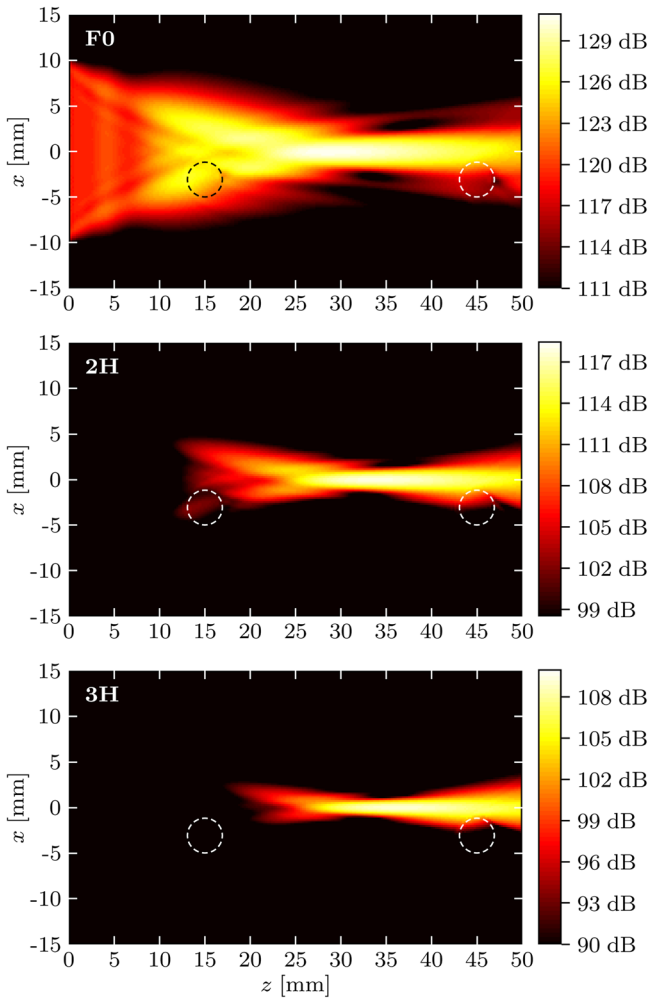

FIG. 6. (Color online) The beam patterns of the harmonics, obtained for the 3D inhomogeneous configuration by the Bi-CGSTAB method with linearization. The scheme is iterated up to $j = 7$ (convergence). Decibel values apply to the maximum field amplitude relative to a pressure of 1 Pa.

$t = 14.3\,\mu$s shows the wave field just after its emission by the transducer. At $t = 22.9\,\mu$s, the reflection from the front of the left inclusion is visible, and at $t = 25.0\,\mu$s the reflections from both the front and the back of the left inclusion can be observed. The maximally focused wave field is shown in the snapshot for $t = 34.3\,\mu$s. At $t = 42.9\,\mu$s, the reflection from the front of the right inclusion is visible.

In the present case, the volume and the contrast of the lossy inclusions cause the Neumann iterative solution (not shown) to strongly diverge, while the Bi-CGSTAB method still yields convergent results. This fact demonstrates the usefulness of the linearization approach.

E. 1D homogeneous configuration and restart strategy

Finally, the configuration of Sec. III A is revisited to study the effect of restarting the relevant iterative scheme. Figure 8 shows the development of the relative error in the harmonics, as obtained for the combination of the Bi-CGSTAB method and a linearized contrast source. This scenario is the same as for the bottom panel of Fig. 2, except

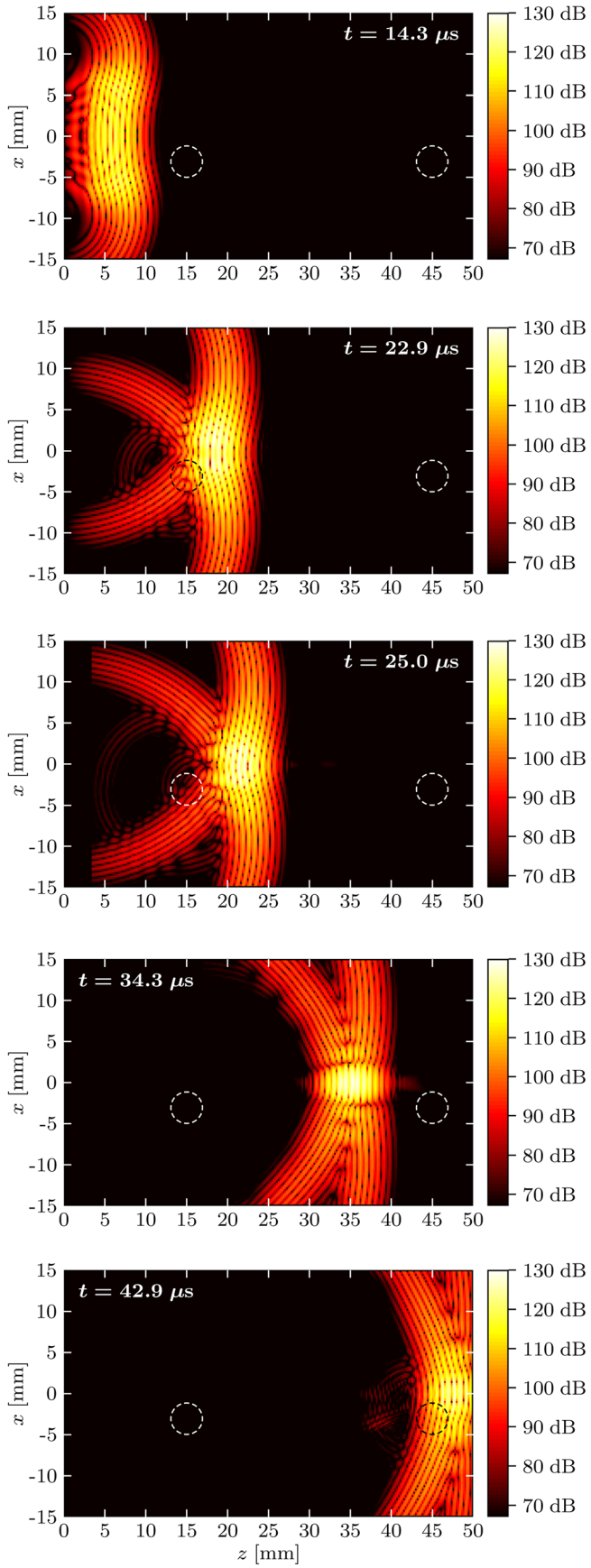

FIG. 7. (Color online) Snapshots of the total nonlinear wave field, obtained for the 3D inhomogeneous configuration by the Bi-CGSTAB method with linearization. The scheme is iterated up to $j = 7$ (convergence). Decibel values apply to the rectified instantaneous field value relative to a pressure of 1 Pa.

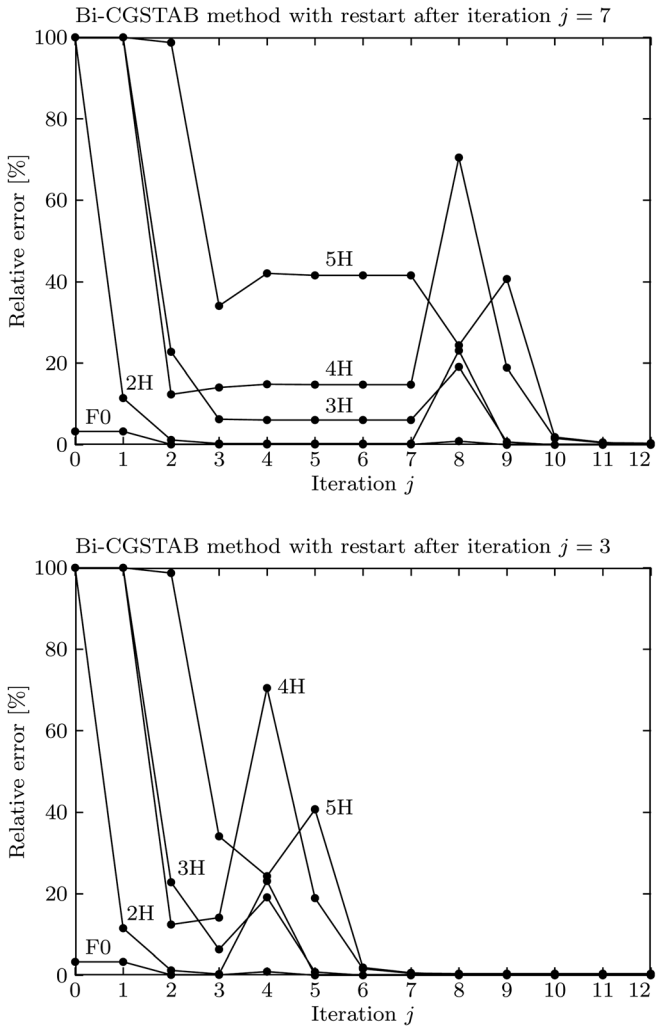

FIG. 8. The relative error in the harmonics obtained for the 1D case by using the Bi-CGSTAB method, a linearized contrast source, and a restart of the scheme after: (top) Seven iterations and (bottom) three iterations. The error is determined with respect to the solution of the Burgers equation.

that now the linearization about $p^{(0)}(\boldsymbol{x}, t)$ is only used up to iteration J, and the subsequent iterations are performed with a linearization about $p^{(J)}(\boldsymbol{x}, t)$.

The top panel of Fig. 8 applies to a restart after iteration $j = 7$. As expected, for iterations $j \leq 7$ the graphs are identical to the ones at the bottom of Fig. 2. Between iterations $j = 4$ and $j = 7$, the errors stay at an almost constant value, indicating that the systematic error due to the linearization about $p^{(0)}(\boldsymbol{x}, t)$ has been arrived at. After iteration $j = 11$, the relative errors stabilize at values that are visually indistinguishable from zero. This shows that the systematic error due to the linearization about $p^{(7)}(\boldsymbol{x}, t)$ is negligible for all the considered higher harmonics.

The bottom panel of Fig. 8 applies to a restart after iteration $j = 3$, which is motivated by the fact that in the top panel there are virtually no developments between iterations $j = 4$ and $j = 7$. Now the relative errors stabilize at vanishingly small values after iteration $j = 7$. This is exactly the same number of iterations needed by the Neumann iterative solution without linearization to reach a vanishingly small error (see the top panel of Fig. 2). It may thus be observed that for the case considered, the restart strategy effectively eliminates the systematic error, while the resulting iterative scheme is as efficient as the original INCS method.

IV. CONCLUSIONS

Linearization of the contrast source term opens a way to apply advanced methods for solving the integral equation of the INCS method and, in turn, to deal with media showing strong inhomogeneities in, e.g., the attenuation.

Numerical results show that the approach works equally well for unsteered and steered beams, i.e., it does not affect the full-wave character of the INCS method. From numerical results it may also be deduced that linearization causes an adverse effect on the convergence rate of the applied solution scheme, which however may be counteracted by choosing an integral equation solver with better convergence properties. In the considered example, a scenario involving the Bi-CGSTAB method and a linearized contrast source converges even faster than a scenario involving the Neumann iterative solution without a linearized contrast source. The linearization causes a systematic error. This error is independent of the chosen integral equation solver, and mainly affects the higher harmonics. The error may effectively be eliminated by restarting the applied iterative scheme with a linearization that is based on the result from the forgoing iterations. In terms of iterations, combining the Bi-CGSTAB method with a linearized contrast source and a restart strategy seems as efficient as the original INCS method. Now that the validity of the linearization approach has been verified, a further extension of the INCS method to deal with media with several inhomogeneous medium parameters, seems opportune.

APPENDIX: LINEARIZATION ABOUT AN ARBITRARY STARTING FIELD

Equations (24)–(26) employ the linearization of $p^2(\boldsymbol{x}, t)$ about the linear primary contribution $p^{(0)}(\boldsymbol{x}, t)$, i.e., the field caused by the primary source $S_{\text{pr}}(\boldsymbol{x}, t)$ in the linear background medium. However, the linearization process may also be performed about any other known field $p^{\text{start}}(\boldsymbol{x}, t)$ that forms a close approximation of the total field $p(\boldsymbol{x}, t)$. In that case

$$p(\boldsymbol{x}, t) = p^{\text{start}}(\boldsymbol{x}, t) + \tilde{p}(\boldsymbol{x}, t), \tag{A1}$$

and it is assumed that

$$\begin{aligned} p^2(\boldsymbol{x}, t) &\approx [p^{\text{start}}(\boldsymbol{x}, t)]^2 + 2p^{\text{start}}(\boldsymbol{x}, t)\tilde{p}(\boldsymbol{x}, t) \\ &= -[p^{\text{start}}(\boldsymbol{x}, t)]^2 + 2p^{\text{start}}(\boldsymbol{x}, t)p(\boldsymbol{x}, t). \end{aligned} \tag{A2}$$

Using this result in Eq. (7), the linearized version of Eq. (21) becomes

$$\begin{aligned} p(\boldsymbol{x}, t) = &p^{(0)}(\boldsymbol{x}, t) + G(\boldsymbol{x}, t) \\ &*_{\boldsymbol{x},t}\{S_{\text{nl}}^{\text{new}}[p(\boldsymbol{x}, t)] + S_{\text{at}}[p(\boldsymbol{x}, t)]\}, \end{aligned} \tag{A3}$$

where

$$S_{\mathrm{nl}}^{\mathrm{new}}(\boldsymbol{x},t)=\frac{\beta}{\rho_0 c_0^4}\partial_t^2\{-[p^{\mathrm{start}}(\boldsymbol{x},t)]^2+2p^{\mathrm{start}}(\boldsymbol{x},t)p(\boldsymbol{x},t)]\}. \tag{A4}$$

Since all contrast sources in Eq. (A3) are linear in $p(\boldsymbol{x}, t)$, this integral equation may again be solved by any appropriate method.

[1]M. A. Averkiou, D. N. Roundhill, and J. E. Powers, "A new imaging technique based on the nonlinear properties of tissues," in *Proceedings of the 1997 IEEE Ultrasonic Symposium*, Toronto, Canada (1997), pp. 1561–1566.

[2]B. Ward, A. C. Baker, and V. F. Humprey, "Nonlinear propagation applied to the improvement of resolution in diagnostic medical ultrasound equipment," J. Acoust. Soc. Am. **101**, 143–154 (1997).

[3]F. Tranquart, N. Grenier, V. Eder, and L. Pourcelot, "Clinical use of ultrasound tissue harmonic imaging," Ultrasound Med. Biol. **25**, 889–894 (1999).

[4]A. Bouakaz, S. Frigstad, F. ten Cate, and N. de Jong, "Super harmonic imaging: A new imaging technique for improved contrast detection," Ultrasound Med. Biol. **28**, 59–68 (2002).

[5]A. Bouakaz and N. de Jong, "Native tissue imaging at superharmonic frequencies," IEEE Trans. Ultrason. Ferroelect. Freq. Control **50**, 496–506 (2003).

[6]P. L. M. J. van Neer, M. G. Danilouchkine, M. D. Verweij, L. Demi, M. M. Voormolen, A. F. W. van der Steen, and N. de Jong, "Comparison of fundamental, second harmonic, and superharmonic imaging: A simulation study," J. Acoust. Soc. Am. **130**, 3148–3157 (2011).

[7]S. B. Feinstein, R. M. Lang, C. Dick, A. Neumann, J. Al-Sadir, K. G. Chua, J. Carroll, T. Feldman, and K. M. Borow, "Contrast echocardiography during coronary arteriography in humans: Perfusion and anatomic studies," J. Am. Coll. Cardiol. **11**, 59–65 (1988).

[8]S. Zhao, M. Borden, S. H. Bloch, D. Kruse, K. W. Ferrara, and P. A. Dayton, "Radiation-force assisted targeting facilitates ultrasonic molecular imaging," Mol. Imaging **3**, 135–148 (2004).

[9]P. N. Burns, D. Hope Simpson, and M. A. Averkiou, "Nonlinear imaging," Ultrasound Med. Biol. **26**, S19–S22 (2000).

[10]P. N. Burns, S. R. Wilson, and D. Hope Simpson, "Pulse inversion imaging of liver blood flow: Improved method for characterizing focal masses with microbubble contrast," Invest. Radiol. **35**, 58–71 (2000).

[11]F. Forsberg, W. T. Shi, and B. B. Goldberg, "Subharmonic imaging of contrast agents," Ultrasonics **38**, 93–98 (2000).

[12]H. J. Vos, D. E. Goertz, and N. de Jong, "Self-demodulation of high-frequency ultrasound," J. Acoust. Soc. Am. **127**, 1208–1217 (2010).

[13]J. H. Ginsberg and M. F. Hamilton, "Computational methods," in *Nonlinear Acoustics*, edited by M. F. Hamilton and D. T. Blackstock (Academic Press, San Diego, CA, 1998), pp. 309–341.

[14]M. D. Verweij and J. Huijssen, "Computational methods for nonlinear acoustic wavefields in homogeneous media," in *Computational Methods in Nonlinear Acoustics: Current Trends*, edited by C. Vanhille and C. Campos-Pozuelo (Research Signpost, Kerala, India, 2011), pp. 1–19.

[15]S. Aanonsen, J. Barkve, J. Naze Tjøtta, and S. Tjøtta, "Distortion and harmonic generation in the near-field of a finite amplitude sound beam," J. Acoust. Soc. Am. **74**, 749–768 (1984).

[16]P. T. Christopher and K. J. Parker, "New approaches to nonlinear diffractive field propagation," J. Acoust. Soc. Am. **90**, 488–499 (1991).

[17]Y.-S. Lee and M. F. Hamilton, "Time-domain modeling of pulsed finite-amplitude sound beams," J. Acoust. Soc. Am. **97**, 906–917 (1995).

[18]J. Tavakkoli, D. Cathignol, R. Souchon, and O. A. Sapozhnikov, "Modeling of pulsed finite amplitude focused sound beams in time domain," J. Acoust. Soc. Am. **104**, 2061–2072 (1998).

[19]R. J. Zemp, J. Tavakkoli, and R. S. C. Cobbold, "Modeling of nonlinear ultrasound propagation in tissue from array transducers," J. Acoust. Soc. Am. **113**, 139–152 (2003).

[20]T. Varslot and G. Taraldsen, "Computer simulation of forward wave propagation in tissue," IEEE Trans. Ultrason. Ferroelectr. Freq. Control **52**, 1473–1482 (2005).

[21]V. A. Khokhlova, A. E. Pomomarev, M. A. Averkiou, and L. A. Crum, "Nonlinear pulsed ultrasound beams radiated by rectangular focused diagnostic transducers," Acoust. Phys. **52**, 481–489 (2006).

[22]P. V. Yuldashev and V. A. Khokhlova, "Simulation of three-dimensional nonlinear fields of ultrasound therapeutic arrays," Acoust. Phys. **57**, 334–343 (2011).

[23]M. F. Hamilton and C. L. Morfey, "Model equations," in *Nonlinear Acoustics*, edited by M. F. Hamilton and D. T. Blackstock (Academic Press, San Diego, CA, 1998), pp. 41–63.

[24]V. W. Sparrow and R. Raspet, "A numerical method for general finite amplitude wave propagation in two dimensions and its application to spark pulses," J. Acoust. Soc. Am. **90**, 2683–2691 (1991).

[25]I. M. Hallaj and R. O. Cleveland, "FDTD simulation of finite-amplitude pressure and temperature fields for biomedical ultrasound," J. Acoust. Soc. Am. **105**, L7–L12 (1999).

[26]S. Ginter, M. Liebler, E. Steiger, T. Dreyer, and R. E. Riedlinger, "Full-wave modeling of therapeutic ultrasound: Nonlinear ultrasound propagation in ideal fluids," J. Acoust. Soc. Am. **111**, 2049–2059 (2002).

[27]J. Hoffelner, H. Landes, M. Kaltenbacher, and R. Lerch, "Finite element simulation of nonlinear wave propagation in thermoviscous fluids including dissipation," IEEE Trans. Ultrason. Ferroelect. Freq. Contr. **48**, 779–786 (2001).

[28]J. Huijssen, "Modeling of nonlinear medical diagnostic ultrasound," Ph.D. thesis, Delft University of Technology, Delft, The Netherlands (2008) pp. 35–128, 171–186, http://repository.tudelft.nl (Last viewed January 6, 2012).

[29]J. Huijssen and M. D. Verweij, "An iterative method for the computation of nonlinear, wide-angle, pulsed acoustic fields of medical diagnostic transducers," J. Acoust. Soc. Am. **127**, 33–44 (2010).

[30]J. Huijssen, M. D. Verweij, and N. de Jong, "Green's function method for modeling nonlinear three-dimensional pulsed acoustic fields in diagnostic ultrasound including tissue-like attenuation," in *Proceedings of the 2008 IEEE Ultrasonic Symposium*, Beijing, China (2008), pp. 375–378.

[31]L. Demi, K. W. A. van Dongen, and M. D. Verweij, "A contrast source method for nonlinear acoustic wave fields in media with spatially inhomogeneous attenuation," J. Acoust. Soc. Am. **129**, 1221–1230 (2011).

[32]L. Demi, N. Ozmen-Eryilmaz, K. W. A. van Dongen, and M. D. Verweij, "Modeling nonlinear pressure fields in inhomogeneous attenuative media using a lossy Green's function and a contrast source," in *Proceedings of 2011 IEEE Ultrasonic Symposium*, Orlando, FL (2011), pp. 2154–2157.

[33]M. D. Verweij and J. Huijssen, "A filtered convolution method for the computation of acoustic wave fields in very large spatiotemporal domains," J. Acoust. Soc. Am. **125**, 1868–1878 (2009).

[34]R. E. Kleinman and P. M. van den Berg, "Iterative methods for solving integral equations," Radio Sci. **26**, 175–181, doi:10.1029/90RS00934 (1991).

[35]P. M. van den Berg and R. E. Kleinman, "Iterative schemes based on minimization of a uniform error criterion," in *PIER 5: Application of Conjugate Gradient Method to Electromagnetics and Signal Analysis*, edited by T. Sarkar (Elsevier, New York, 1991), pp. 27–65.

[36]R. E. Kleinman and P. M. van den Berg, "Iterative methods for solving integral equations," in *PIER 5: Application of Conjugate Gradient Method to Electromagnetics and Signal Analysis*, edited by T. Sarkar (Elsevier, New York, 1991), pp. 67–102.

[37]J. T. Fokkema and P. M. van den Berg, *Seismic Applications of Acoustic Reciprocity* (Elsevier, Amsterdam, The Netherlands, 1993), pp. 41–61.

[38]B. J. Landsberger and M. F. Hamilton, "Second-harmonic generation in sound beams reflected from, and transmitted through, immersed elastic solids," J. Acoust. Soc. Am. **109**, 488–500 (2001).

[39]Y. Du and J. A. Jensen, "Feasibility of non-linear simulation for Field II using an angular spectrum approach," in *Proceedings of the 2008 IEEE Ultrasonics Symposium*, Beijing, China (2008), pp. 1314–1317.

[40]Y. Jing, M. Tao, and G. T. Clement, "Evaluation of a wave-vector-frequency-domain method for nonlinear wave propagation," J. Acoust. Soc. Am. **129**, 32–46 (2011).

[41]F. Varray, A. Ramalli, C. Cachard, P. Tortoli, and O. Basset, "Fundamental and second-harmonic ultrasound field computation of inhomogeneous nonlinear medium with a generalized angular spectrum method," IEEE Trans. Ultrason. Ferroelect. Freq. Contr. **58**, 1366–1376 (2011).

[42]B. E. Treeby, J. Jaros, A. P. Rendell, and B. T. Cox, "Modeling nonlinear ultrasound propagation in heterogeneous media with power law absorption using a *k*-space pseudospectral method," J. Acoust. Soc. Am. **131**, 4324–4336 (2012).

[43]L. Demi, M. D. Verweij, J. Huijssen, N. de Jong, and K. W. A. van Dongen, "Attenuation of ultrasound pressure fields described via a contrast source formulation," in *Proceedings of 2009 IEEE Ultrasonics Symposium*, Rome, Italy (2009), pp. 1590–1593.

[44]N. Ozmen-Eryilmaz, L. Demi, E. J. Alles, M. D. Verweij, and K. W. A. van Dongen, "Modeling acoustic wave field propagation in 3D breast models," in *Proceedings of 2011 IEEE Ultrasonics Symposium*, Orlando, FL (2011), pp. 1700–1703.
[45]M. D. Verweij, "Modeling space-time domain acoustic wave fields in media with attenuation: The symbolic manipulation approach," J. Acoust. Soc. Am. **97**, 831–843 (1995).
[46]M. D. Verweij, "Transient acoustic wave fields in continuously layered media with depth-dependent attenuation: An analysis based on higher-order asymptotics," J. Acoust. Soc. Am. **101**, 1808–1820 (1997).
[47]In a previous work of the current authors, the function $m(t)$ appeared as $\chi(t)$.
[48]P. N. T. Wells, "Absorption and dispersion of ultrasound in biological tissue," Ultrasound Med. Biol. **1**, 369–376 (1985).
[49]F. A. Duck, *Physical Properties of Tissue* (Academic Press, London, UK, 1990), pp. 99–123.
[50]J. C. Bamber, "Ultrasonic properties of tissues," in *Ultrasound in Medicine*, edited by F. A. Duck, A. C. Baker, and H. C. Starritt (Institute of Physics, Bristol, UK, 1998), pp. 73–76.
[51]L. B. Felsen and N. Marcuvitz, *Radiation and Scattering of Waves* (IEEE Press, New York, 1994), pp. 1–9.
[52]T. L. Szabo, "Causal theories and data for acoustic attenuation obeying a frequency power law," J. Acoust. Soc. Am. **97**, 14–24 (1995).
[53]H. A. van der Vorst, "Bi-CGSTAB: A fast and smoothly converging variant of Bi-CG for the solution of nonsymmetric linear systems," SIAM (Soc. Ind. Appl. Math.) J. Sci. Stat. Comput. **13**, 631–644 (1992).
[54]D. T. Blackstock, M. F. Hamilton, and A. D. Pierce, "Progressive waves in lossless and lossy fluids," in *Nonlinear Acoustics*, edited by M. F. Hamilton and D. T. Blackstock (Academic Press, San Diego, CA, 1998), pp. 65–150.